

Programmable Anti-Aliasing Filter Design

Nicolas Alarcon (na2946), Claire Cizdziel (ctc2156), ELEN E4215 Fall 2024

Abstract—We designed a digitally programmable low-pass anti-aliasing filter (AAF) using a 6th-order Ackerberg-Mossberg topology, powered by dual 1V supplies with a total power consumption of approximately 1.493mW. The filter has 2-bit control to program the passband response (Butterworth or Chebyshev) and to select the 3dB cutoff frequency (150kHz or 300kHz). Using 2-to-1 analog multiplexers, we efficiently switched between resistor values, while maintaining functionality with only three biquadratic filter stages. The design prioritized low power consumption, utilizing a single-pole op-amp behavioral model with a second stage gain of 100V/V, a DC open-loop gain of 200V/V, and capacitance constraints of 500fF. This resulted in a slew rate of $55 \frac{V}{\mu s}$, a maximum output current (I_{max}) of $27.6\mu A$, and a transconductance (gm) of $138.2 \frac{\mu A}{V}$.

I. INTRODUCTION

For low-power active-RC designs, biquadratic filters (biquads) offer an effective solution, as the elements of the transfer function often correspond directly to component ratios within the biquad. In this course, we covered various biquad topologies, including Tow-Thomas, Ackerberg-Mossberg (AM), and several single-amplifier designs. We chose the Ackerberg-Mossberg topology despite its requirement of three op-amps per stage, because single-amplifier biquads tend to exhibit high sensitivity to resistor value variations, making them harder to manufacture reliably, especially in high-Q systems. Additionally, we avoided the Tow-Thomas biquad due to its higher phase error compared to the AM topology.

To implement four different low-pass filters using only three stages of AM biquads, we incorporated a 4-to-1 analog multiplexer (MUX) composed of two 2-to-1 MUXes. This allowed us to switch between component values while accounting for parasitics with a 100Ω resistor at each 2-to-1 MUX input. The filter specifications are shown in Table I, with a 5% accuracy constraint on all component values.

TABLE I
TARGET ANTI-ALIASING FILTER SPECIFICATIONS

Parameter	Specification	Description
Passband Response	Butterworth & Chebyshev	Programmable passband characteristic
Cutoff frequency	150kHz/300kHz	Filter 3dB frequency
DC gain	0 dB	
Filter Order	6th Order	
Maximum Input Amplitude	500mV	Peak Signal Amplitude
Average (DC) Input Level	0V	

II. TRANSFER FUNCTION DERIVATION

A. Butterworth Transfer Function Derivation

The required transfer functions for a N-th Order Butterworth low pass filter takes the form of

$$H(s) = \frac{\omega_0^N}{(s-p_1)(s-p_2)\dots(s-p_N)}. \quad (1)$$

for a passband maximum attenuation (α_{max}) of 3dB. The poles locations p_k are derived from (2) where $\omega_0 = 2\pi f_p$ and $\varepsilon \approx 1$ for a passband maximum attenuation of 3dB (3).

$$p_k = \sigma_k + j\omega_k = -\omega_0[\sin\psi_k + j\cos\psi_k] \quad (2)$$

where $\psi_k = \frac{\pi(2k-1)}{2N}$ and k = 1 to N

$$\omega_0 = \omega_p(\varepsilon)^{-\frac{1}{N}} \text{ and } \varepsilon = \sqrt{10^{\alpha_{max}/10} - 1} \quad (3)$$

For a 3-stage biquad with a DC Gain of 0dB, this results in a transfer function

$$H(s) = \frac{\omega_0^2}{s^2 + (\omega_0/Q_1)s + \omega_0^2} \frac{\omega_0^2}{s^2 + (\omega_0/Q_2)s + \omega_0^2} \frac{\omega_0^2}{s^2 + (\omega_0/Q_3)s + \omega_0^2} \quad (4)$$

where Quality Factors Q_1 , Q_2 , and Q_3 are ordered from least to greatest in order to prevent clipping for high-Q stages and Q_k results from

$$Q_k = \frac{\omega_{0k}}{2|\sigma_k|} \text{ and } \omega_{0k} = \sqrt{\sigma_k^2 + \omega_k^2}. \quad (5)$$

The 150kHz and 300kHz coefficients and Q values are as follows in Table II.

TABLE II
IDEAL BUTTERWORTH TRANSFER FUNCTION COEFFICIENTS

Passband Frequency	Stage	w0 (rad/s)	w0^2	Qk	w0/Qk
150kHz	1	9.42E+05	9.42E+05	5.18E-01	1.82E+06
	2	9.42E+05	9.42E+05	7.07E-01	1.33E+06
	3	9.42E+05	9.42E+05	1.93E+00	4.88E+05
300kHz	1	1.88E+06	3.55E+12	5.18E-01	3.64E+06
	2	1.88E+06	3.55E+12	7.07E-01	2.67E+06
	3	1.88E+06	3.55E+12	1.93E+00	9.77E+05

These calculations were verified in Matlab with the above transfer function, with the three stages cascaded.

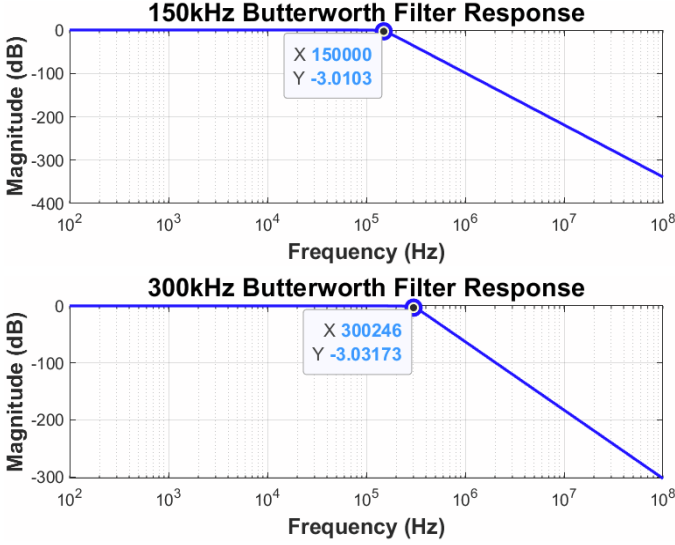


Fig. 1. Butterworth Magnitude Frequency Responses

B. Chebyshev Transfer Function Derivation

The required transfer functions for a N-th Order Chebyshev low pass filter take the form of

$$H(s) = \frac{w_p^N}{\varepsilon^{2^{N-1}}(s-p_1)(s-p_2)\dots(s-p_N)}. \quad (6)$$

where $\varepsilon \approx 1$ for $\alpha^{\max} = 3\text{dB}$ (3), and the poles locations p_k can be found from

$$p_k = \sigma_k + j\omega_k \quad (7)$$

$$= -\omega_p [\sinh(a) \sin \psi_k + j \cosh(a) \cos \psi_k]$$

where $\psi_k = \frac{\pi(2k-1)}{2N}$, $k = 1$ to N , and $a = \frac{1}{N} \sinh^{-1}(\frac{1}{\varepsilon})$

For a 3-stage biquad with a DC Gain of 0dB, this results in a transfer function

$$H(s) = \frac{\omega_{01}^2}{s^2 + (\omega_0/Q_1)s + \omega_{01}^2} \cdot \frac{\omega_{02}^2}{s^2 + (\omega_0/Q_2)s + \omega_{02}^2} \cdot \frac{\omega_{03}^2}{s^2 + (\omega_0/Q_3)s + \omega_{03}^2} \quad (8)$$

where ω_{0k} and Q_k result from (5).

The 150kHz and 300kHz coefficients and Q values are as follows in Table III.

TABLE III

IDEAL CHEBYSHEV TRANSFER FUNCTION COEFFICIENTS

Passband Frequency	Stage	w0k (rad/s)	w0k^2	Qk	w0k/Qk
150kHz	1	2.81E+05	7.89E+10	1.04E+00	2.69E+05
	2	6.81E+05	4.64E+11	3.46E+00	1.97E+05
	3	9.21E+05	8.48E+11	1.28E+01	7.21E+04
300kHz	1	5.62E+05	3.16E+11	1.04E+00	5.38E+05
	2	1.36E+06	1.85E+12	3.46E+00	3.94E+05
	3	1.84E+06	3.39E+12	1.28E+01	1.44E+05

These calculations were also verified in Matlab with the above transfer function, with the three stages cascaded.

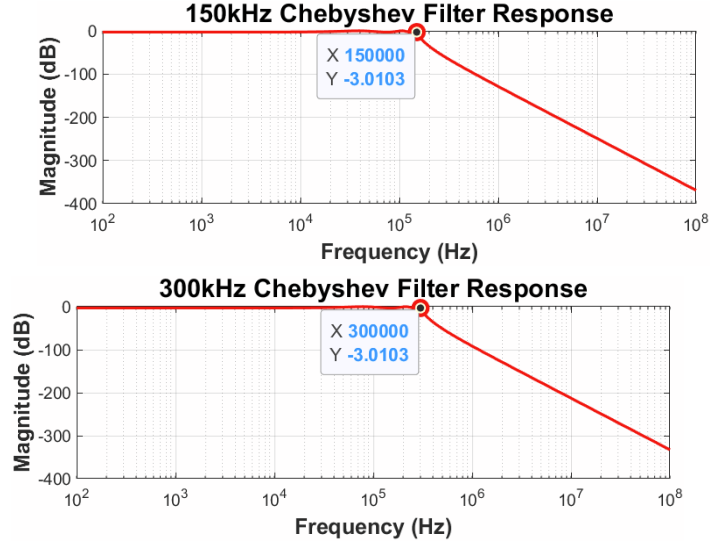


Fig. 2. Chebyshev Magnitude Frequency Responses

III. BUILDING THE ANALOG MULTIPLEXER

To facilitate efficient switching between the four filter types, we built a 4-to-1 MUX to select between them based on the logic levels at $Vsel0$ and $Vsel1$ (Figure 3).

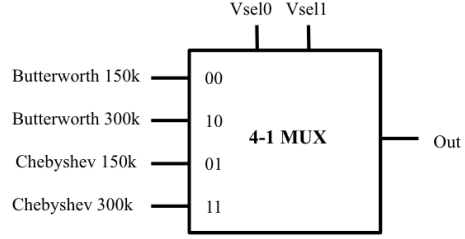


Fig. 3. 4-to-1 MUX diagram for Programming 4 Filters

To simulate this multiplexer, we first designed a 2-to-1 MUX, shown in Figure 4. This schematic uses $1\text{m}\Omega$ resistors in series with an *ahdlib* switch.

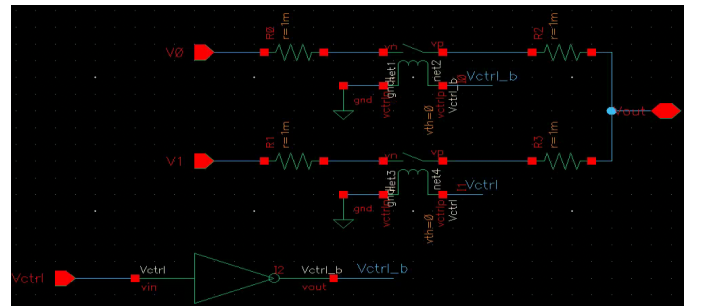


Fig. 4. 2-to-1 MUX Schematic

By arranging the 2-to-1 MUX as a symbol and cascading it in two stages, we achieved a functional 4-to-1 MUX, shown in Figure 5. The 4-to-1 MUX schematic selects one of four inputs based on the combination of the two selection inputs using three 2-to-1 MUXes. Each input has a series 100Ω resistor to limit current and improve switching stability.

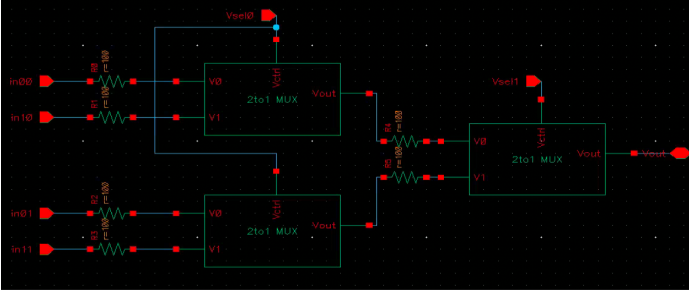


Fig. 5. 4-to-1 MUX Schematic

To control our MUX selections, we connected two voltage sources across the V_{sel0} and V_{sel1} control signals throughout the filter. By setting the voltage of V_{sel0} and V_{sel1} to either 0V or 1V, we were able to select and test each filter configuration (Figure 6).

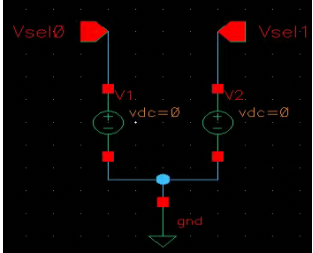


Fig. 6. Voltage switching schematic for V_{sel0} and V_{sel1}

IV. DESIGN OF FILTER

The design of our digitally programmable low-pass AAF filter was based on an op-amp RC topology. Since the filter is 6th-order, we began by constructing a three-stage Ackerberg-Mossberg filter, as shown in Figure 7.

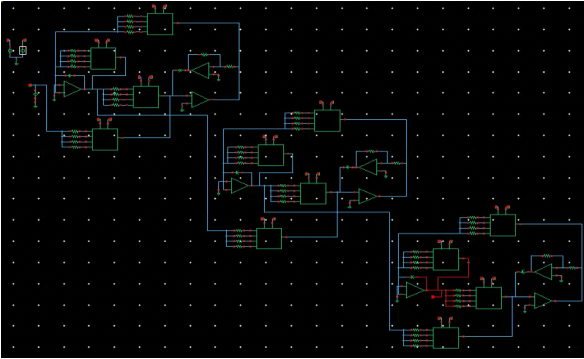


Fig. 7. Programmable AAF Filter Schematic Overview

To accommodate the four possible filter configurations (combinations of passband response and cutoff frequency), we replaced each resistor (R_A' , R_A ', R_B ', R_2) in the topology with

the previously developed 4-to-1 MUX. Using the derived and verified transfer functions, we calculated the appropriate resistor values and integrated them into the filter. These calculations were conducted using the standard equation (9) for AM filter component values.

$$H_1(s) = -\frac{\frac{1}{R_2 R_A C_A C_A'}}{s^2 + s \frac{1}{R_B C_A} + \frac{1}{R_A R_A' C_A C_A'}}$$
(9)

Using our desired low pass filter functionality, this equation can be simplified to obtain the component values required. All R_1 values were infinity and C_1 values 0pF.

$$R_A = R_A' = \frac{1}{w_0 C_A}$$
(10)

$$R_B = R_A Q_1$$
(11)

These component values were implemented into the filter, and all calculated values are shown in Table VI. Each set of resistors (R_A' , R_A ', R_B ', R_2), for the respective filters was

connected to the MUX in its corresponding location. The MUX selection bits (V_{sel0} and V_{sel1}) were set to 00, 01, 10, or 11 through a voltage source, determining which resistor values were activated in the filter. All capacitances were set to an arbitrary value of 250pF. Additionally, the resistors in the inverting op-amp stage of the topology were fixed at a constant value of 10k Ω for signal inversion. The final design of the three stages is shown below in Figures 8-10, a closer look at Figure 7.

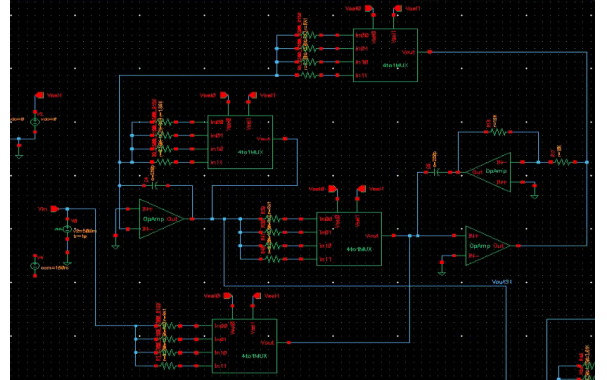


Fig. 8. Programmable AAF Filter, Stage 1

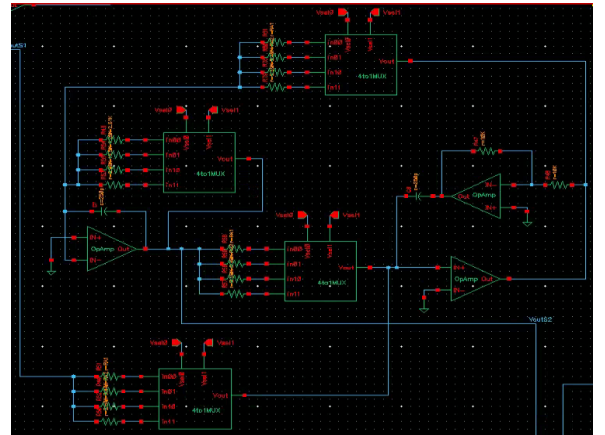


Fig. 9. Programmable AAF Filter, Stage 2

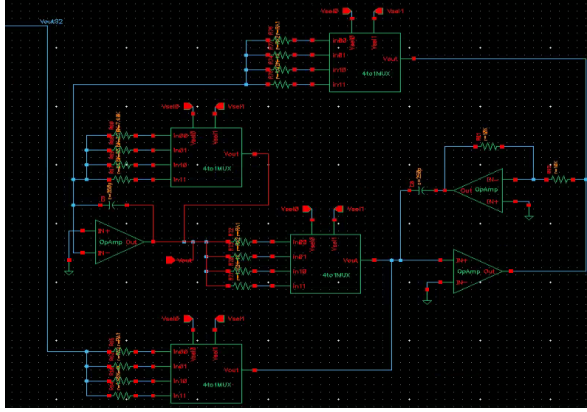


Fig. 10. Programmable AAF Filter, Stage 3

V. PRACTICAL OP-AMP MODEL

A. Op-amp Design

The filter is specified to have op-amp subcomponent requirements of $I_{omax}/g_m = 200mV$ and output stage limited to $\pm 800mV$ output swing. To integrate this into our larger filter, we began with a simple sub-circuit with a voltage-controlled voltage source (vcvs) with a gain of 1000V/V (Figure 11).

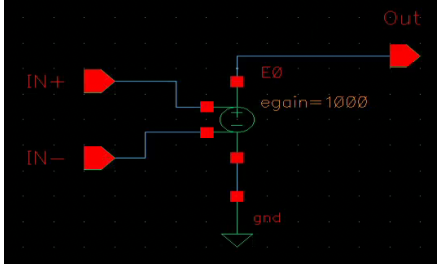


Fig. 11. Simple Op-amp Sub-circuit

We used this idealized simple op-amp to verify standard operation of our AM filter topology. We then developed a practical op-amp sub-circuit that would meet the specifications of our filter. We calculated the slew rate ($\max V_o \omega_0$) of each stage of each filter in Table IV. Slew rate is calculated by multiplying the frequency response and ω_0 . Using MATLAB, we ran an AC sweep of the transfer function and determined the $V_o \omega_0$ peak of each stage. This gave us the required slew rate for each filter type, of which we took the maximum. Then, we cascaded the previous stage, as the input of the next stage to find the maximum possible slew rate of filters and stages as shown in Figure 12. We repeated this for the second and third stages.

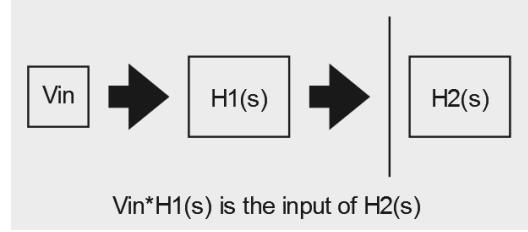


Fig. 12. Slew Rate Input Calculation Method

TABLE IV
SLEW RATES OF EACH FILTER STAGE

	Filter	Frequency	Slew Rate
Stage 1	Butterworth	150k	4.88E+05
	Butterworth	300k	2.44E+05
	Chebyshev	150k	1.47E+05
	Chebyshev	300k	2.93E+05
Stage 2	Butterworth	150k	4.10E+05
	Butterworth	300k	2.05E+05
	Chebyshev	150k	2.30E+05
	Chebyshev	300k	4.58E+05
Stage 3	Butterworth	150k	7.52E+05
	Butterworth	300k	3.76E+05
	Chebyshev	150k	6.23E+05
	Chebyshev	300k	1.28E+06

From this process of calculations, we obtained the maximum slew rate to use, as highlighted in yellow. However, when we initially targeted the minimum slew rate, the DC open-loop gain was too low, at approximately 1V/V. To address this, we set a DC gain target (A_{DC}) of 200V/V, with the second stage gain (A_2) set to 100V/V, while reducing the op-amp bandwidth to minimize power consumption. Power consumption was estimated at $6V \times I_{omax}$ per op-amp, with 3 op-amps in each biquad. We initially set the first pole location (f_{p1}) to 300kHz, experimentally decreasing it to about 220kHz, after which it negatively impacted the transfer function with peaking near the passband frequency. With a Miller capacitance (C) of 500fF, we arrived at the final op-amp specifications and operating parameters, as shown in Table V using the following relations:

$$R = \frac{1}{2\pi f_{p1} C A_2} \quad (12)$$

$$g_m = 2\pi f_{p1} C A_{DC} \text{ and } \frac{I_{omax}}{g_m} = 200mV \quad (13, 14)$$

$$\text{Op-Amp Unity Gain Frequency } f_u = \frac{g_m}{2\pi C}. \quad (15)$$

$$\text{DC Closed Loop Variation} = \left(\frac{A_{DC}}{1+A_{DC}} - 1 \right) * 100\%. \quad (16)$$

$$\text{Expected Slew Rate} = \frac{I_{omax}}{C} \quad (17)$$

The power consumption of nine total op-amps is:

$$\text{Total Power Consumption} = 54V * I_{omax}. \quad (18)$$

TABLE V
PRACTICAL OP-AMP SPECS

Op-amp specs	gm	1.38E+04
	R	1.45E+04
	lomax	2.76E-05

Power Consumption	1.493	mW
Op-amp Unity Gain Freq.	4.40E+07	
Slew Rate	55.29	V/us
Unity Gain Closed Loop Variation	0.49	%

The application of these calculations to the practical model is illustrated in Figure 13. We first tested the functionality of the op-amp independently before integrating it into the larger filter schematic.

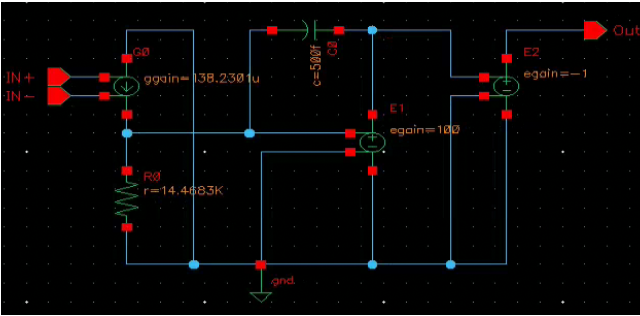


Fig. 13. Practical Op-amp Sub-circuit

B. Practical Op-amp Testing and Verification

We began by testing the DC and AC performance. The DC sweep confirmed a slope/gain of 200V/V, as observed in Figure 14. The AC response showed a DC gain of 46.02dB (about 200V/V), with a -3dB point at 217.36kHz, a 0dB point at 43.84MHz, and a phase shift of -45° at 219.24kHz. All these values aligned with our expectations (Figure 15). In this response, the gain is represented in purple, and the phase is shown in green.

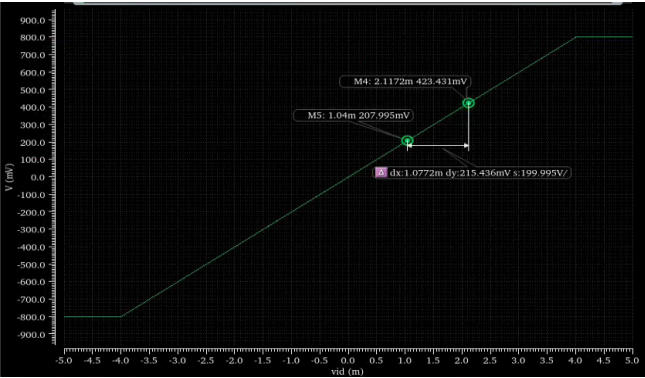


Fig. 14. Op-amp DC Sweep Simulation

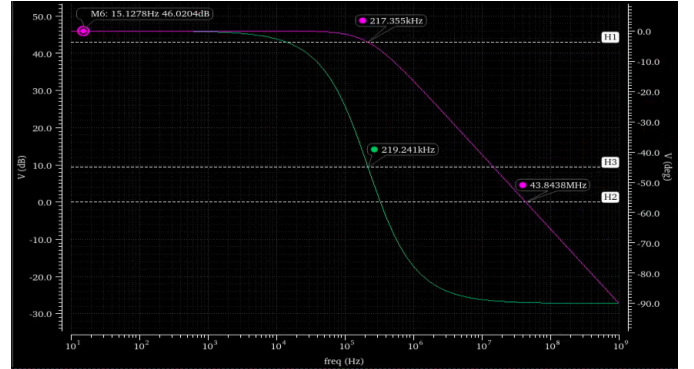


Fig. 15. Op-amp AC Response Simulation

We conducted these DC and AC simulations with the following configuration in Figure 16.

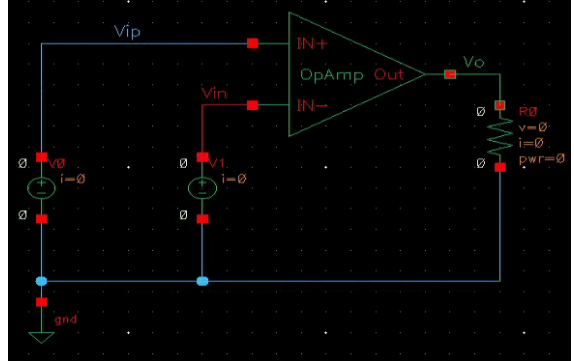


Fig. 16. DC and AC Simulation Op-amp Configuration

Next, we tested the slew rate of our model using a transient simulation. The output transient slope, which corresponds to the slew rate, was found to be 54.46MV/s, in line with our expectations (Figure 17). In this response, V_{in} is shown in red and V_{out} in green.

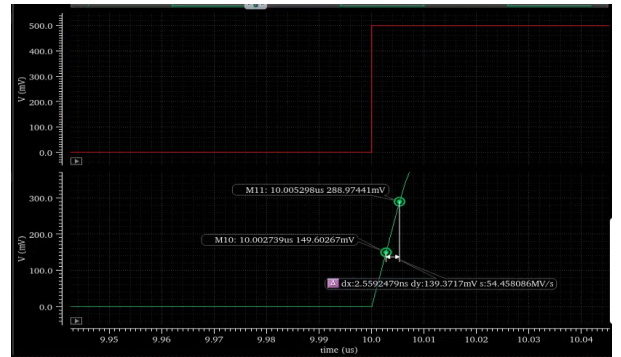


Fig. 17. Op-amp Transient Response Simulation

We conducted this transient simulation with the following configuration in Figure 18.

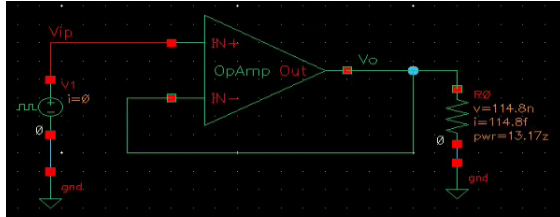


Fig. 18. Transient Simulation Op-amp Configuration

With the functional practical op-amp confirmed, we replaced all ideal op-amps in the filter schematic with this model and conducted further testing to ensure accurate frequency response.

VI. FILTER TESTING AND VERIFICATION

A. Determining Filter Component Values

To verify the functionality of our filter with the practical op-amp, we analyzed the AC response magnitude using a 500mV input voltage to ensure accurate cutoff frequency. During this analysis, we found that our initial resistor calculations did not achieve the desired cutoff frequency within a 5% tolerance. This discrepancy was due to the parasitics introduced by the 100Ω resistors added to each stage of the 4-to-1 MUX. To compensate for these parasitics, we reduced all calculated resistor values by 200Ω . While this adjustment showed some improvement, the responses were still outside the 5% cutoff frequency tolerance. As a result, we recalculated the resistor values to target a cutoff frequency slightly higher than the desired value, allowing the parasitics to bring the frequency to the intended value. For the Butterworth filters at 150kHz and 300kHz, and the Chebyshev filter at 300kHz, we calculated for a +10kHz shift in cutoff. For the Chebyshev filter at 150kHz, we used a +5kHz shift, as a +10kHz shift led to a cutoff frequency that was too high. The comprehensive list of all component values used is shown in Table VI.

TABLE VI

INITIAL AND FINAL FILTER COMPONENT VALUES

Butterworth 150k			
Original Calculations			
Q	0.518	0.707	1.93
Stage 1	4.24	4.24	4.24
RA ($k\Omega$)	2.2	3	8.19
R2 ($k\Omega$)	4.24	4.24	4.24
Final Values			
RA ($k\Omega$)	3.78	3.78	3.78
RB ($k\Omega$)	1.86	2.61	7.48
R2 ($k\Omega$)	3.78	3.78	3.78

Butterworth 300k			
Original Calculations			
Q	0.518	0.707	1.93
Stage 1	2.12	2.12	2.12
RA ($k\Omega$)	1.1	1.5	4.1
R2 ($k\Omega$)	2.12	2.12	2.12
Final Values			
RA ($k\Omega$)	1.85	1.85	1.85
RB ($k\Omega$)	0.864	1.25	3.76
R2 ($k\Omega$)	1.85	1.85	1.85

Chebyshev 150k			
Original Calculations			
Q	1.044	3.458	12.78
Stage 1	14.2	5.88	4.34
RA ($k\Omega$)	14.9	20.3	55.5
R2 ($k\Omega$)	14.2	5.88	4.34
Final Values			
RA ($k\Omega$)	13.6	5.49	4
RB ($k\Omega$)	14.2	19.5	53.5
R2 ($k\Omega$)	13.6	5.49	4

Chebyshev 300k			
Original Calculations			
Q	1.044	3.458	12.78
Stage 1	7.12	2.94	2.17
RA ($k\Omega$)	7.43	10.2	27.8
R2 ($k\Omega$)	7.12	2.94	2.17
Final Values			
RA ($k\Omega$)	6.28	2.59	1.92
RB ($k\Omega$)	6.56	8.96	24.5
R2 ($k\Omega$)	6.28	2.59	1.92

B. Verifying Filter Functionality with Simulations

Figure 19 shows the response of each of the four filters, with each filter labeled by color on the left-hand side, increased in size on the graph for readability. The phase response was also simulated and is shown in Figure 209.

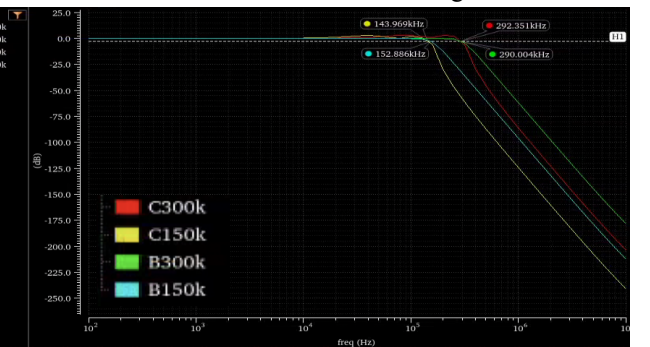


Fig. 19. Filter AC Response Simulation, Magnitude

Table VII, shows each filter's response, all within the $\pm 5\%$ the expected value.

TABLE VII
FILTER AC RESPONSE CUTOFF FREQUENCY VALUES

Filter	Frequency	Cutoff Freq
Butterworth	150k	152.89kHz
Butterworth	300k	290.00kHz
Chebyshev	150k	143.97kHz
Chebyshev	300k	292.35kHz

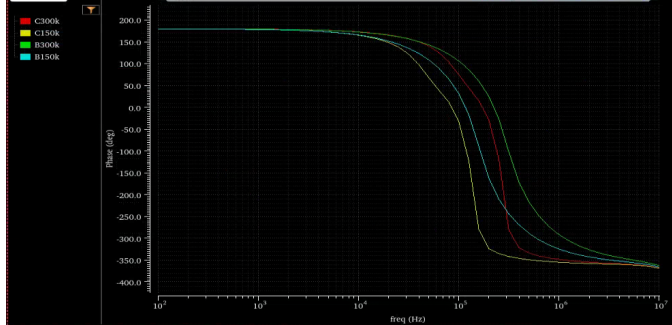


Fig. 20. Filter AC Response Simulation, Phase

We anticipated a DC gain of 0dB, which all filters were close to. Specifically, B150k had a gain of 333.86 dB, B300k gain of 332.92 dB, C150k gain of 115.54 dB, and C300k gain of 115.94 dB. As these values are in the milli dB range, the filters are operating as anticipated. We also conducted transient simulations to determine slew rates (Figure 21).

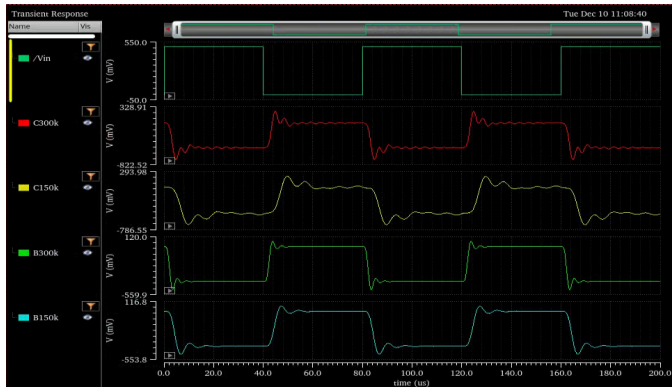


Fig. 21. Filter Transient Response Simulation

The slew rate for each filter was calculated from the slope of the linear region of the transient response. This was derived as shown in Figure 22, where we determined the slew rate of the Butterworth 150k filter. This method was replicated to obtain all slew rate values shown in Table VIII.

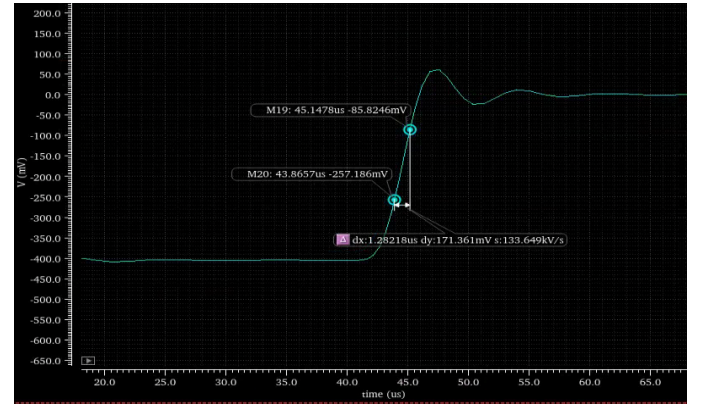


Fig. 22. Butterworth 150k Slew Rate Derivation

TABLE VIII
TRANSIENT RESPONSE SLEW RATE VALUES

Filter	Frequency	Slew Rates
Butterworth	150k	133.65kV/s
Butterworth	300k	266.08kV/s
Chebyshev	150k	163.77kV/s
Chebyshev	300k	336.45kV/s

VII. CONCLUSION

We designed and implemented a digitally programmable low-pass anti-aliasing filter. Through detailed simulations and testing, we verified the functionality of the filter and ensured it met desired specifications and our hand calculations. Adjustments to resistor values were made to account for parasitics, and performance was evaluated across various filter configurations. Our results demonstrate achieving the targeted frequency response and low power consumption, showing a suitable solution for practical applications.